Effect of Nanostructured Microporous Surfaces on Pool Boiling Augmentation

Gheitaghy, Amir Mirza; Saffari, Hamid; Zhang, Guo Qi

Important note
To cite this publication, please use the final published version (if applicable).
Please check the document version above.

Effect of Nanostructured Microporous Surfaces on Pool Boiling Augmentation

Amir Mirza Gheitaghy, Hamid Saffari & Guo Qi Zhang

Submit your article to this journal ⬈

View Crossmark data ⬈

Taylor & Francis
Taylor & Francis Group

Check for updates

Effect of Nanostructured Microporous Surfaces on Pool Boiling Augmentation

Amir Mirza Gheitaghy[a,b], Hamid Saffari[a], and Guo Qi Zhang[b]

[a]School of Mechanical Engineering, Iran University of Science and Technology, Tehran, Iran; [b]Department of Microelectronics, Delft University of Technology, Delft, the Netherlands

ABSTRACT

Nanostructured microporous surfaces were electrodeposited at various electrolyte temperatures on copper substrate to investigate the saturated pool boiling enhancement of distilled water at atmospheric pressure. Surface structure topography and wickability were analyzed to investigate their relation to critical heat flux. Scanning electron microscope showed that the micro-clusters have nanostructures from cubic at 5°C to dendritic at 60°C electrolyte temperature. Rate-of-rise experiments demonstrated that dendritic copper structure has the best capillary performance. The experimental results of pool boiling heat transfer indicate that the critical heat flux increased with surface wickability. Electrodeposited porous surface in hot electrolyte showed the highest critical heat flux and heat transfer coefficient of the 124 W/cm^2 and 17 W/cm^{2}K, respectively, which is 50% and 270% higher than that of plain surface. However, the two-step electrodeposition and annealing were used in fabrication of surfaces, but the mechanical strength of layer needs more improvement by changing the electrochemical process parameters.

Introduction

Boiling heat transfer can provide an extremely high heat transfer coefficient under a low superheat condition due to the latent heat of the working fluid during phase transition process; this is recognized as an effective way for cooling high power devices. Demand from higher power generation, lower equipment size, and process efficiency improvement has led to extensive research on the enhancement of heat transfer performance. It is widely accepted that surface structures play a crucial role in the enhancement of pool boiling. Several studies [1] were conducted to identify the effective parameters of surface roughness [2], [3], wettability [4], [5], and porosity [6], [7] for optimized pool boiling performance. Experimental results show that hydrophilic porous surfaces have best performance in enhancing the boiling curve [8]. This enhancement can be attributed to a variety of mechanisms, including increased nucleation site densities at lower wall superheat [9], increased bubble departure frequency [10], enhanced micro-convection around nucleated bubbles [11], elongated triple contact line [12], and enhanced microlayer evaporation via a wicking effect [13]. Among these possible mechanisms, the enhanced microlayer evaporation through wicking has been widely accepted as the dominant mechanism

for critical heat flux (CHF) enhancement, and correlations [14] and theoretical predictions [15] have been established between the CHF and the wicking rate. For a bubble nucleated on a solid surface during boiling, evaporation occurs both along the apparent liquid–vapor interface and the microlayer near the bubble contact line, where nanostructure-enhanced liquid delivery through wicking stabilizes the evaporating thin film, thereby improving the CHF. Increasing the surface area and roughness by nanostructures can enhance hydrophilicity and wicking of surfaces. In order to better understand enhanced boiling heat transfer mechanism, the effect of the micro/nanostructures on the wicking phenomena needs to be studied.

Different kinds of nanostructured microporous surfaces have been used in heat transfer enhancement studies, and these structures have resulted in dramatic augmentation of heat transfer [16], [17]. Rioux et al. [18] systematically studied surfaces created from nanostructure by acid etching to microscale by a sintering process. Results showed that using hierarchical multiscale modulated porous surfaces have led to the most significant improvements of 350% in heat transfer coefficient (HTC) and 200% in CHF over the polished plain surface. Chu et al. [19] fabricated hierarchically

structured surfaces, using electrophoretic deposition of silica nanoparticles on microstructured silicon and electroplated copper microstructures covered with copper oxide nanostructures. A CHF of $\approx 250\,\text{W/cm}^2$ was achieved on a CuO hierarchical surface with a roughness factor of 13.3. Nazari and Saedodin [20] used an electrochemical process of anodizing to coat an aluminum oxide layer on aluminum plain surface. They found porous nanostructured coatings, due to their improved surface characteristics particularly wettability, increased CHF values by about 80% in comparison to the plain surface. Patil et al. [21] reported that a significant enhancement in HTC of 17.9 $\text{W/cm}^2\text{K}$ was obtained from a copper chip with cauliflower-like morphology fabricated by a two-step electrodeposition process. Xu et al. [22] fabricated a composite copper porous surface by electrochemical deposition. Experimental results revealed that the HTC of the porous surface was 120% higher than that of the plain surface. Li et al. [23] fabricated a well-ordered 3D macro-porous metallic surface layer with nanostructured porosity by the electrochemical method, and pool boiling heat transfer experiment with R134a indicated that the heat transfer coefficient was enhanced by over a favor of 17 compared to a plain reference surface. Tang et al. [24] adopted a method of hot-dip galvanizing/dealloying to fabricate a nanoporous structure on copper surface, and found a reduction of 63% in wall superheat and an increase of 172% in heat transfer coefficient compared with the nonstructure. Tetreault-Friend et al. [25] used layer-by-layer deposition charged solutions of nanoparticles and polymers to investigate effects of pore size and porous layer thickness on the CHF. Experimental data support the hypothesis that CHF is governed by the competition between capillary wicking, viscous pressure drop and evaporation, as well as conduction heat transfer within the porous layer. Gao et al. [26] demonstrated that surface structure of nanoporous copper prepared by electrodeposition and heat treatment can improve the bonding strength by 77%, decrease the wall superheat by 45%, and increase the HTC by 80%. Lu et al. [27] used a dealloying process to nanostructure formation and visualization results showed a higher bubble departure frequency, higher active nucleation site density, and lower probability for bubble merging, all cause boiling enhancement. Gheitaghy et al. [28] used two-step electrodeposition with high current density of 250 mA/cm^2 for a short time (50 seconds) and obtained 1.6 and three fold CHF and HTC enhancement, respectively over the plain surface.

In this paper, two-step electrochemical deposition of copper is used at various electrolyte temperatures to fabricate the hydrophilic microporous surfaces with different nanostructures. The temperature parameter is used due to its 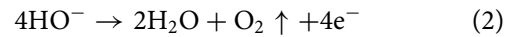impact on nanostructure morphology and there is a dearth of literature on it. The effect of electrolyte temperature on structures are investigated from scanning electron microscope (SEM) images. Wickability of structures is measured with capillary rate-of-rise experiments and its effect on CHF is examined. Saturated pool boiling is carried out on three samples to compare the enhancement relative to polished copper and predictions are proposed according to wickability performance.
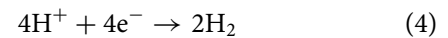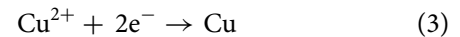
Experimental method

Samples fabrication by electrodeposition method

Electrodeposition is an electrochemical process of ion reduction at the cathode by passing direct current through the solution (galvanostatic). As shown in Figure 1(a_2), circular polished copper with diameter of 22 mm was used as the cathode and a copper cylinder with larger area was used as the anode. The two electrode surfaces were fixed parallel 3 cm apart in the stationary solution. Two simultaneous reduction reactions for the Cu^{2+} and H^+ ions in the electrolyte solution happen at the cathode as soon as the electric current is supplied to the electrochemical deposition cell:

Anode:

$$Cu \rightarrow Cu^{2+} + 2e^- \tag{1}$$

$$4HO^- \rightarrow 2H_2O + O_2 \uparrow + 4e^- \tag{2}$$

Cathode:

$$Cu^{2+} + 2e^- \rightarrow Cu \tag{3}$$

$$4H^+ + 4e^- \rightarrow 2H_2 \tag{4}$$

In the anode, copper loses electrons to form copper ions. In the cathode, the copper ions obtain the electrons and are redeposited as copper again. Simultaneously, there is hydrogen production as shown in Figure 1(a_1). The rapidly generated bubbles partly occupy the volume of the copper deposit sediment, leaving a porous surface with multi-scale structure. Figure 1 shows the similarity between the hydrogen bubble template in electrodeposition process and vapor bubble in pool boiling experiment on electrodeposited copper. Since formation of the structure is directed by continuous dynamic gas bubbles, the structure can facilitate the escape of the gas bubbles generated from the surface. Therefore, such porous surface structure can be more suitable to use in gas generation processes such as boiling where the bubbles need to be quickly dissipated from the surface.

Two-step electrochemical deposition is carried out in an electrolyte solution of $CuSO_4$ (0.4 M) and H_2SO_4 (1.5 M), subjected to high current density (600 mA/cm^2) for 100 seconds followed by lower current density
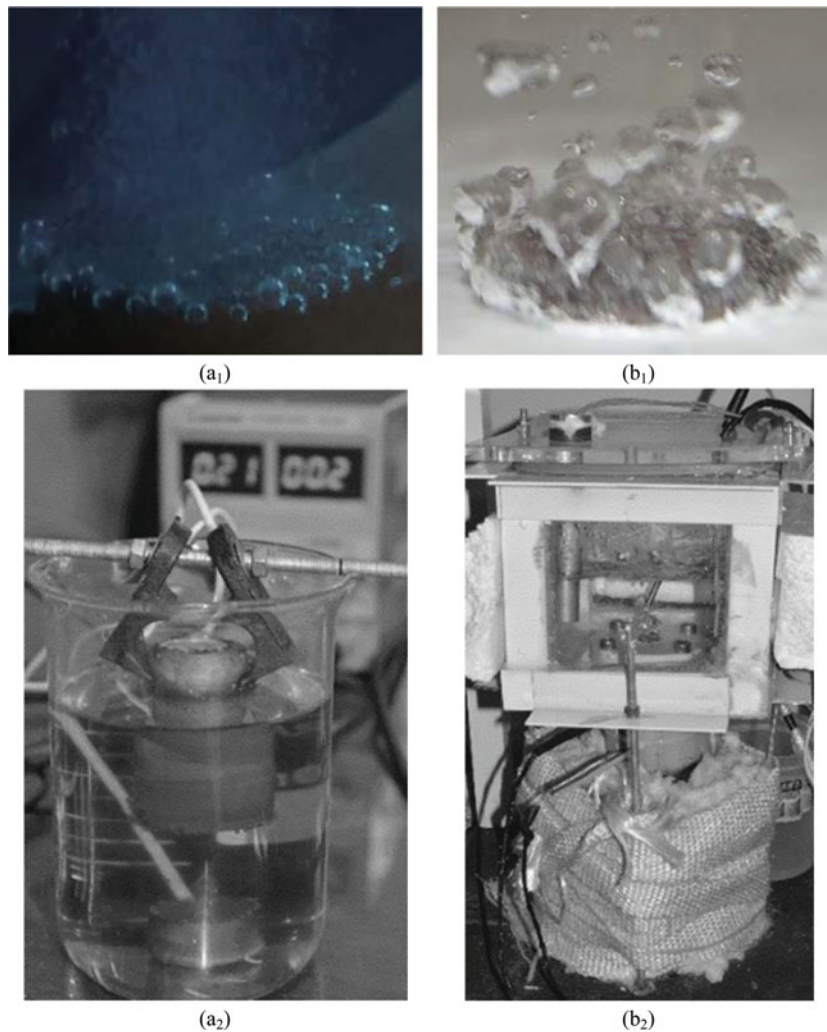
Figure 1. Similarity between (a_1) hydrogen bubbles in (a_2) electrodeposition process, and (b_1) vapor bubbles in (b_2) pool boiling process.

(60 mA/cm^2) for 2,500 seconds. A series of porous surfaces were prepared under different electrolyte temperatures of 5, 30, and 60°C.

Pool boiling experiment

Pool boiling experiments were carried out using the experimental setup (Figure 2) presented in author's previous research [29] with water at atmospheric pressure on three electrodeposited samples and polished copper to investigate the effect of micro/nanostructures on pool boiling performance. The experimental facility consisted of the heating module, the power supply module, the boiling vessel, the data collection module, and the visualization module. The heating module consisted of cartridge heater, copper block, and copper rod sample. Cartridge heater embedded in the copper block was used to provide heat to the surface. Copper rod sample was fixed to copper block by a Polytetrafluoroethylene cone frustum. Teflon was selected to fix the copper rod sample due to its excellent processing ability and low heat conductivity coefficient. The layout ensures the electrodeposited copper is exposed to the pool liquid. The data collecting module included four K-type thermocouples, a data acquisition unit, and a computer. The arrangement of thermocouples is such that an estimate of the heat flux could be obtained from three thermocouples (of 0.5 mm diameter) that were located at the center of the copper rod sample with 15 mm intervals. Also, the wall temperature could be determined based on a linear temperature distribution and the measurement by a thermocouple that is placed 3 mm below the heat transfer surface. The samples are circular copper disks and microporous structures are fabricated on their top surface. The sample size (or the boiling area) was 4 cm^2, which was large enough to eliminate edge effects and show a similar boiling behavior to an infinite boiling surface. The sample was surrounded by Polyetheretherketone (PEEK) and the space where the heater block was located was evacuated for thermal insulation. PEEK is a thermoplastic that has a large thermal resistance and is compatible with an aqueous chemical environment.

Before the experiment, de-ionized water was charged into the chamber. The distance between the liquid level and surface was set as 150 mm. Auxiliary heaters were
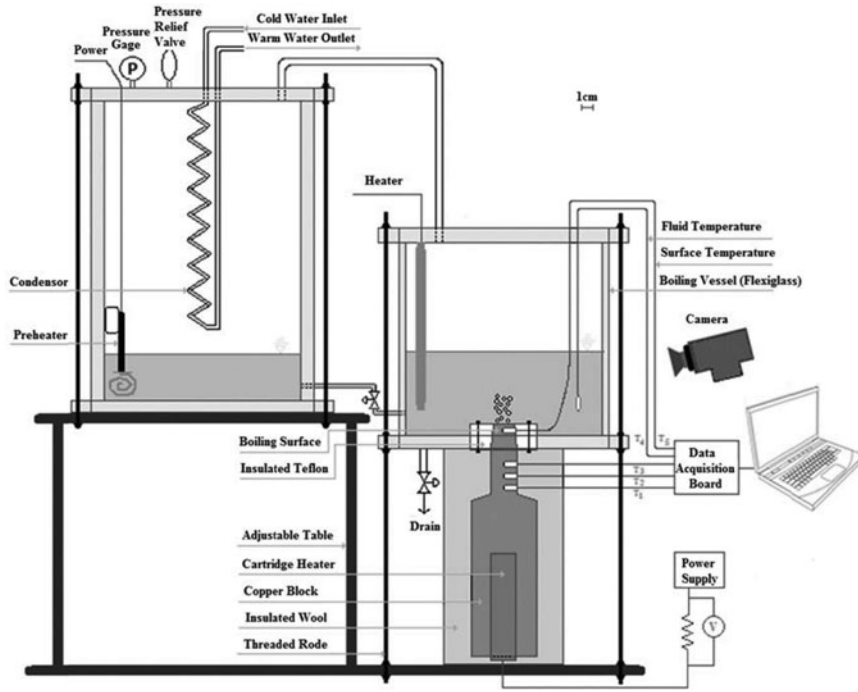
Figure 2. Pool boiling experimental setup.

turned on to boil the liquid for 1 hour to remove noncondensable gases. During the experiment, the temperature of the working fluid was kept at saturation temperature and the temperature fluctuation of the working fluid was less than 0.2°C. The heat transfer was considered to have reached a steady state if the variation of the wall temperature was smaller than 0.1°C after about 10 minutes and the same steps were repeated at each heat flux. The uncertainty of the measured heat flux was mainly dependent on the accuracy of the position and calibration of the thermocouples. The maximum uncertainties in measurement were about 13% for the heat flux and 6% for temperature [29]. Verification and comparison of the pool boiling curve on the polished surface with literature has been presented in our previous research [28].

CHF prediction by considering wettability and wickability

Among a variety of hypothetical explanations to understand the boiling enhancement, explanations which relate the CHF to the wettability and wickability have been recently presented in the literature [30]–[32]. Wetting is the ability of a liquid to maintain contact with a solid surface, and the degree of wetting (wettability) is determined by a force balance between adhesive and cohesive forces which are measured by droplet contact angle. Wicking is the ability to sustain the capillary flow and wickability is a transportation of liquid from one place to another driven by capillary action which is measured by liquid absorption. Wetting is a prerequisite for wickability, as a liquid that does not wet the porous layer cannot wick into

it. Highly wettable and wickable surface can be obtained with high surface energy materials that strengthen surface energy by micro/nanostructures.

Kandlikar [33] reported the analytical CHF model for saturated pool boiling of pure liquid on horizontal heater with the effect of wettability as follows:

$$q''_{\text{Kandlikar}} = h_{\text{fg}}\rho_{\text{g}}{}^{0.5} \left(\frac{1 + \cos\beta}{16} \right) \left[\frac{2}{\pi} + \frac{\pi}{4}(1 + \cos\beta)\cos\emptyset \right]^{0.5} [\sigma g(\rho_{\text{l}} - \rho_{\text{g}})]^{0.25} \quad (5)$$

where h_{fg} is the latent heat, ρ_{g} and ρ_{l} are the density of the vapor and liquid, respectively, β is the contact angle, $\emptyset$ is the surface orientation, g is the gravity acceleration, and σ is the surface tension.

Ahn et al. [30] discussed the effect of the capillary wicking of the micro/nanostructures on the CHF enhancement in the spreading region, because liquid spreading on modified surfaces is generated due to the capillary wicking. They found that CHF increases more than the prediction of Kandlikar on plain surface. Therefore, they modified Eq. (5) for CHF prediction with the effect of capillary wicking as follows:

$$q''_{\text{CHF}} = q''_{\text{Kandlikar}} + q''_{\text{gain}} \quad (6)$$

Heat flux gain due to capillary wicking is proportional to absorbed liquid volume as below [20]:

$$q''_{\text{gain}} = \frac{\rho_l h_{fg} \dot{V}}{A_{\text{heating}}} \quad (7)$$

where $\dot{V}$ is the volumetric flow rate of supplied liquid by capillary wicking, and A_{heating} is the area of the heating surface. Volumetric flow rate can be calculated as follows:

$$\dot{V} = \frac{d\left(\varepsilon\delta A_{\text{wetted}}\right)}{dt} = \varepsilon\delta\frac{dA_{\text{wetted}}}{dt} \tag{8}$$

where A_{wetted}, ε, and δ are the area wetted by capillary wicking, the porosity of structured surface, the thickness of structure, respectively. The porosity and the thickness of modified structures can be estimated using SEM images. dA_{wetted}/dt indicates the initial (maximum) time differential term of the wetted area, and it is determined through visualization of the capillary wicking action at the moment of liquid suction. The wicked volume flow rate captures the effects of micro/nanostructure size, morphology, permeability, intrinsic contact angle, and porosity all into one phenomenological parameter. This technique yields a direct measurement of the actual mass flow rate, and allows for a direct correlation with CHF via the additional latent heat associated with the wicked liquid mass flow.

Results and discussion

Morphology and characteristics

Figure 3 shows differing magnification SEM images of electrodeposited copper surface morphology for three electrolyte temperatures. For the surface prepared at the coldest temperature of 5°C, nanocube grains clustered to form a nonuniform bi-porous interconnected structure. As the electrolyte temperature increases to 60°C, the grains turned to dendritic branches and the clusters connected more uniformly to form a hole with diameter of about 100 μm. This may be attributed to the decreasing viscosity and surface tension of electrolyte with increasing the temperature [34]. Decreasing the viscosity decreases the concentration polarization around the cathode surface and it causes the growth of dendritic grains on the cathode surface. Also, it facilitates the transport of detached hydrogen bubbles through the interior of the deposit, thus forming a channel structure through it. The decrease of surface tension of the solution lowers the break-off diameter and increases the quantity of hydrogen bubbles, although the net mass of generated gas is proportional to electrolyte molarity and current density and temperature has a negligible effect on it. In comparison with electrodeposited structure made by Patil et al. [21] in higher copper sulfate concentration (0.8M) and lower deposition time (15 seconds), the uniform porous layer with higher thickness fabricated. Also, in comparison with author's previous work [28] current density of 250 mA/cm^2 for 50 seconds, the mechanical stability was weaker and nanostructures depend on electrolyte temperature.

Mechanical stability of the structures is one of the important issues in using porous structures for two-phase
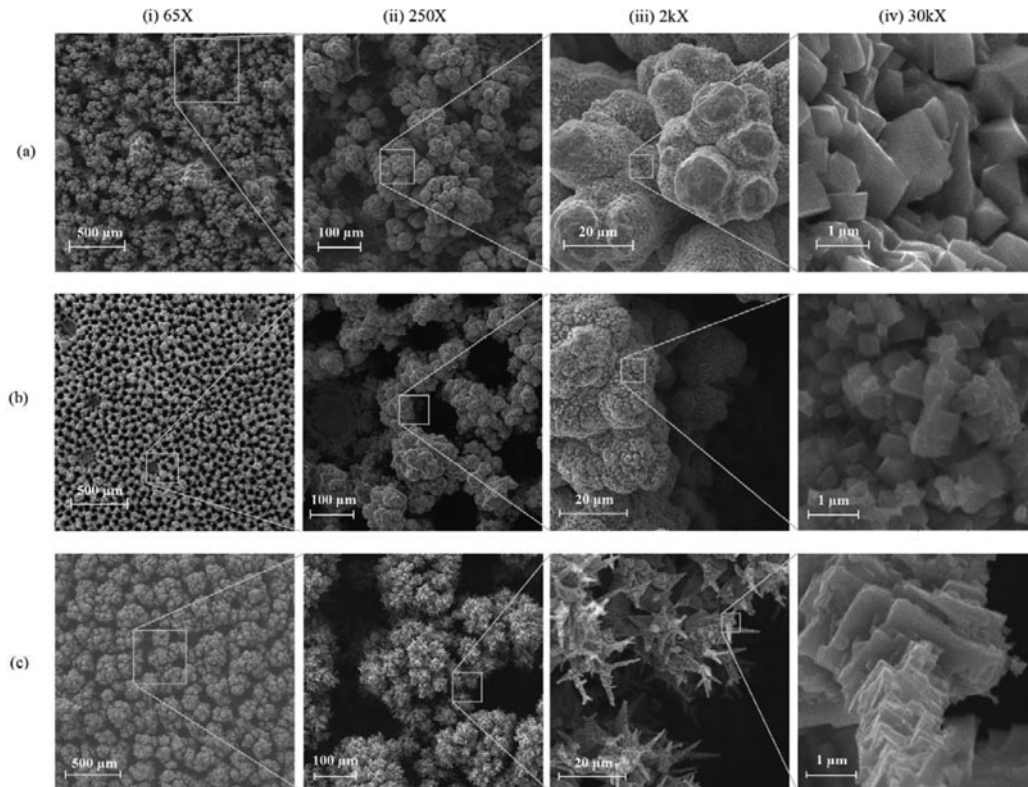

Figure 3. SEM images of micro/nanostructured copper synthetized in different electrolyte temperatures of (a) 5°C, (b) 30°C, and (c) 60°C.
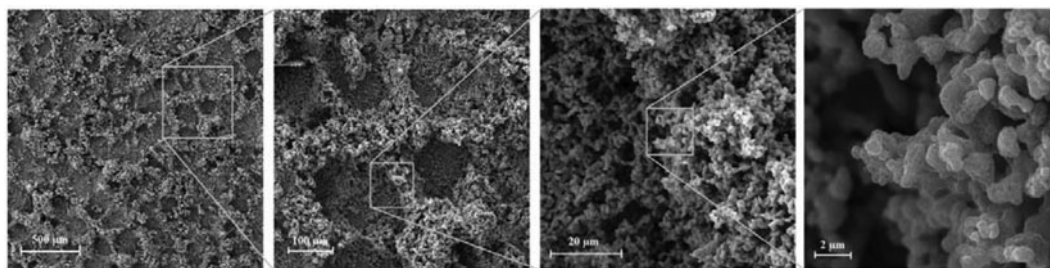
Figure 4. SEM images of annealed copper (one-step electrodeposited at 30°C electrolyte temperature) at 500°C for 2 hours.
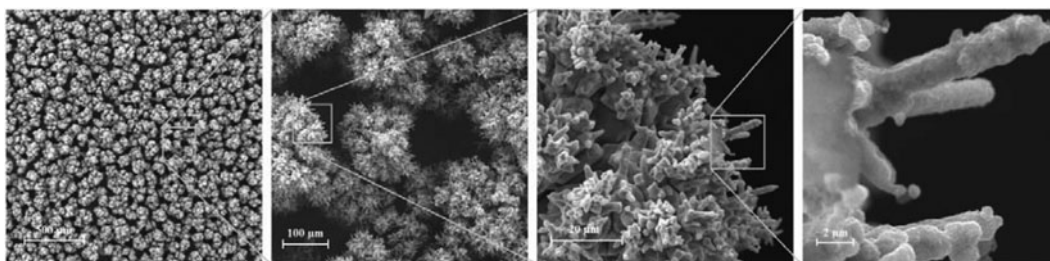

Figure 5. SEM images of annealed dendritic copper (two-step electrodeposited prepared at 60°C electrolyte temperature) at 500°C for 2 hours.

heat transfer. Two usual approaches for stability improvement of electrodeposited porous structures are annealing and multi-step electrodeposition. Microstructure at the end of the first step electrodeposition is highly porous, but fragile and delicate to handle. In the second step, the very low rate of deposition of the Cu atoms strengthens the microstructure by filling up the open macropores and barely changes the thickness and surface morphology. Figure 4 shows the annealed one-step electrodeposition sample which has not formed completely or with requisite stability. Then, two-step electrodeposition is used but nanodendritic structures are still brittle. Therefore, annealing at a relatively high temperature (500°C) for few hours (2 hours) under reducing conditions (50% H_2 + 50% N_2) is applied to further improve stability. Figure 5 shows the SEM images of a dendritic electrodeposited sample prepared in 60°C electrolyte temperature after annealing. The macro-scale structure remains unchanged (pore size, thickness), but nanostructures change due to the melting of high energy surfaces. However, the surface area of the structure is reduced, while the stability is improved.

CHF prediction

In order to predict the CHF of surfaces according to Eq. (6), the required parameters need to be determined. Selected frames of the capillary rate-of-rise experiment captured as a function of time for one sample have been shown in Figure 6. These are used to determine the wetting area according to time in three samples. Surface samples are oriented perpendicular to the horizontal surface of a liquid reservoir. Once the sample base touches the reservoir surface, the liquid rises along the surface due to a finite capillary pressure gradient. The location of the rising liquid front is tracked as a function of time.

The wetted area is calculated by tracking the displacement of the water front on the surface. Figure 7 shows the wetted area in samples and initial (maximum) flow rate compute according to 2 seconds of initial wicking. There is a slight difference between samples electrodeposited at 5°C and 30°C, while the data at 60°C shows a higher initial slope and more wicking ability due to dendritic nanostructures and high effective surface area.

The thickness of samples prepared in electrolyte temperature of 5, 30, and 60°C, are 300, 270, 220 μm, respectively. The porosity of samples shown in Figure 8 are determined with area estimation by ImageJ software. The porous surface electrodeposited at 30°C has the greatest porosity of 67%.

The CHF for polished copper with receding contact angle of 70° was predicted by Kandlikar's correlation [33] to be 91.7 W/cm² and agreed well with current experiments. The required parameters for CHF estimation of porous structures electrodeposited in different electrolyte temperatures are presented in Table 1. Based on these predictions for the samples shown the porous surface electrodeposited in 60°C temperature has a maximum wicked flow rate and it is expected that the CHF of this surface be 19.9 W/cm² more than Kandlikar's prediction.

Pool boiling performance

Pool boiling experiments were conducted to investigate heat transfer enhancement in saturated nucleate boiling of de-ionized water under atmospheric pressure on polished
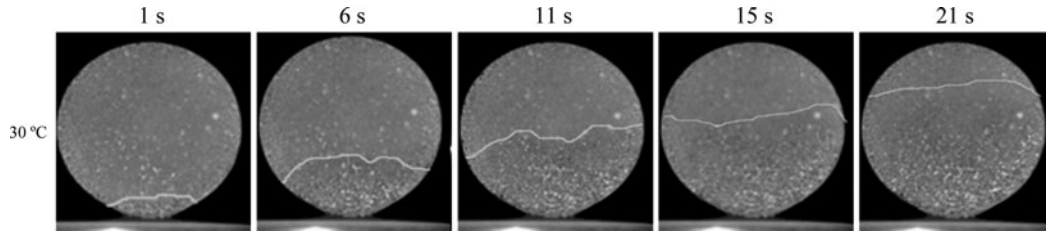
Figure 6. Selected frame of capillary rate-of-rise experiment of sample prepared at 30°C electrolyte temperature.
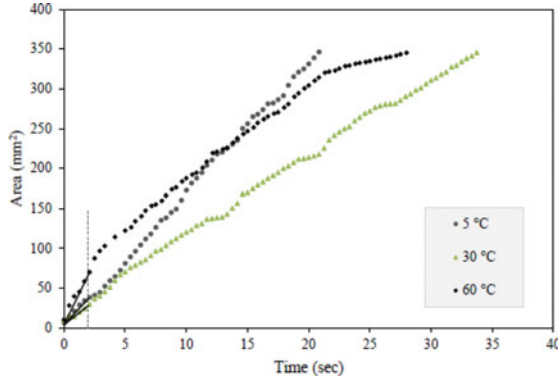

Figure 7. Capillary rise area as a function of time for electrodeposited samples in different electrolyte temperatures.

and nanostructured microporous surfaces. Figure 8 shows pool boiling data of nanostructured microporous coatings electrodeposited at 30°C and 60°C electrolyte temperatures, polished copper, and Rohsenow's correlation.

Experiments were conducted on plain polished copper as a reference surface. The plain copper surface was polished with a #2500 grit sandpaper and its roughness was measured to be 0.2 μm. Rohsenow [35] recognized the influence of the liquid solid combination on boiling heat transfer and developed a generalized correlation:

$$\frac{c_p \Delta T_s}{h_{fg}} = C_{sf} \left[\frac{q''}{\mu h_{fg}} \sqrt{\frac{\sigma}{g \left(\rho_l - \rho_g \right)}} \right]^{0.33} \left(\frac{c_p \mu}{k} \right)_l^m \quad (9)$$

where ΔT_s is the superheat temperature, q'' is the heat flux, m is the empirical constant with a value of 1.7 as suggested by Rohsenow [35]. The empirical constant C_{sf} takes care of the solid-liquid combination and value of 0.0085 has been taken to match with the result. Comparisons of the present boiling data with Rohsenow's correlation are shown in Figure 9.

The microporous surface electrodeposited at 5°C was destroyed during the pool boiling experiment due to weak adhesion between structure and substrate. As shown in Figure 9a, the microporous surfaces resulted in significantly lower wall superheats than polished surface under the same heat flux condition. For example, when the heat flux was 50 W/cm^2, the reduction in wall superheat of the microporous was 60% of the polished surface. At the stage of incipient boiling, wall superheat of the microporous surfaces was around 2.5 K, whilst that of a polished surface was 7.8 K. Experimental data on maximum heat flux confirmed that wickability is an effective explanation; and qualitatively, the surface with more ability to absorb liquid can reach a higher heat flux. The hollow data points show the prediction of CHF according to wickability on
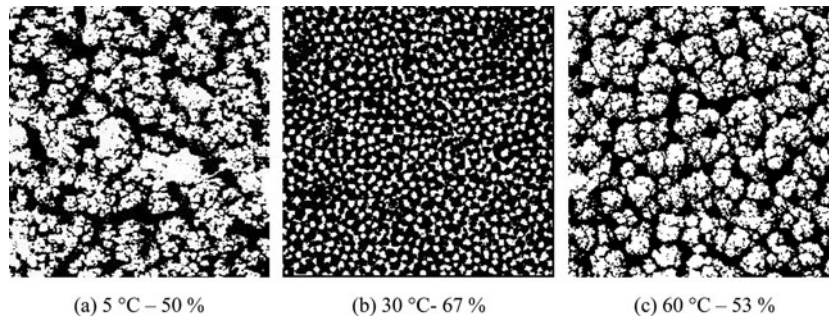

Figure 8. Porosity determination of samples with ImageJ software.

Table 1. Parameters of porous structures electrodeposited in different electrolyte temperatures.

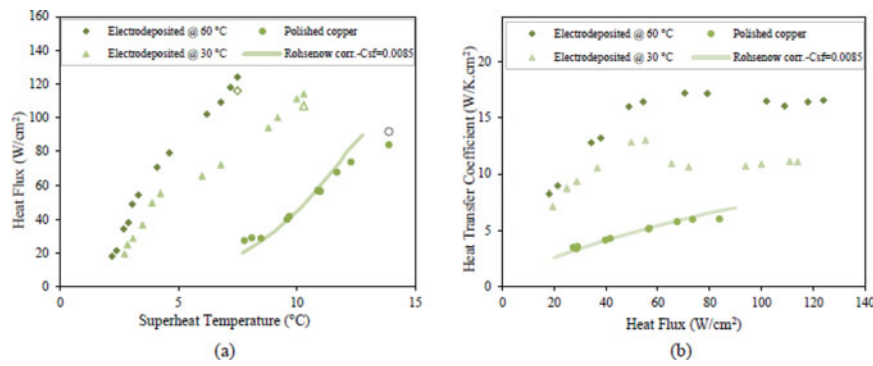| Electrolyte temperature of prepared samples	Porosity	Thickness (μm)	dA_{wetted}/dt (mm^2/s)	$\dot{V}$ (mm^3/s)	q''_{gain} (W/cm^2)	q''_{CHF} (W/cm^2)
5°C	0.50	300	19	2.8	17.4	109.1
30°C	0.67	270	14	2.5	15.4	107.1
60°C	0.53	220	34	3.9	24.2	115.9

Figure 9. Comparison of (a) pool boiling curve, (b) heat transfer coefficient for electrodeposited samples and polished copper.

microporous surfaces and Kandlikar's prediction on polished surface. They are slightly lower than data obtained experimentally. Lower prediction of CHF on microporous surfaces may be due to the base of porous media, which may result in faster liquid absorption underneath the surface that, however, could not be observed. In addition, there are uncertainties in determination of each parameter in Eq. (8), in order to predict the gained heat flux of wicked liquid. The enhancement of the CHF observed in the microporous coatings appears to be the result of the capillary surface rewetting and thermal thin-film evaporation.

Dependence of HTC on heat flux is presented in Figure 9b. The HTC of microporous surfaces is higher than that of polished surface at any measured heat flux. At low to moderate heat flux conditions ($<60 \text{ W/cm}^2$), microporous surfaces show excellent heat transfer enhancement. Microporous structures with more wickability appear to provide more liquid to evaporate from thin films inside porous structure, accelerate bubble generation and frequency with more active nucleation sites at lower superheat, decreasing bubble diameter because of porous boundaries and increasing the heat transfer area. With the increase of heat flux, the advantage of microporous surfaces for nucleate boiling heat transfer performance declines. At moderate to high heat flux ($>60 \text{ W/cm}^2$), bubbles generated on the microporous surface coalesce into bigger clusters or even form into a vapor film near the porous surface which increases the thermal resistance. More wickability helps to maintain a wetted surface despite higher vapor production and quickly replenishes the heated surface with cold liquid after local evaporation leading to re-wetting of dry patches and consequently delaying the CHF.

The porous surface electrodeposited at high electrolyte temperature showed the maximum CHF of 124 W/cm² and the best HTC of 17 W/cm²K which was 1.5 and 3.7 times than that of the polished surface, respectively. However, the mechanical stability of these porous surfaces needs improvement for long-term use.

Conclusions

An experimental study has been undertaken to investigate pool boiling heat transfer performance of electrodeposited nanostructured microporous surfaces which were fabricated in electrolyte temperature of 5, 30, 60°C. The following conclusions may be drawn:

1. Through the surface morphology analysis and pool boiling experiment, it is known that by selecting the electrodeposition parameters such as electrolyte temperature, different nanostructured microporous surfaces with better boiling performance can be obtained.

2. Two-step electrodepostition and annealing can improve binding to the substrate and structural strength of the porous layer. However, stability of porous structures should be considered when long-term application is evaluated.

3. Surface prepared at 60°C electrolyte temperature, with dendritic nanobranch in micropores, can increase the HTC by 270% and decrease the wall superheat by 60%, which implies that the nanoporous structure plays an important role in promoting the development of enhanced boiling heat transfer technology.

4. According to the CHF prediction by wickability analysis, the nanostructured microporous surface with more liquid absorption ability can delay the dry-out and deviation from experimental results was less than 20%.

Nomenclature

A_{wetted}	wetted area, m²
A_{heating}	boiling area, m²
c_p	heat capacity, j/kg. K
C_{sf}	liquid-surface constant in Rohsenow's correlation
CHF	critical heat flux
$CuSO_4$	copper sulfate
g	gravitational acceleration, m/s²

h_{fg} latent heat, j/kg

H_2SO_4 sulfuric acid

HTC   heat transfer coefficient

k   thermal conductivity, W/m.k

m   empirical constant in Rohsenow's correlation

q'' heat flux, W/m^2

SEM   scanning electronic microscope

T temperature, °C

t time, s

ΔT_s wall superheat temperature, °C

$\dot{V}$ volumetric flow rate, m^3/s

Greek symbols

β dynamic receding contact angle, °

ρ density, kg/m^3

ε Porosity, dimensionless

μ liquid dynamic viscosity, kg/m.s

$\varnothing$ surface orientation, °

δ thickness, μm

σ surface tension, N/m

Subscripts

g   gas

l   liquid

Notes on contributors

Amir Mirza Gheitaghy is a former Ph.D. candidate in mechanical engineering at Iran University of Science and Technology. His research interests include two-phase heat transfer, nanofluid, and nanoscale heat conduction. He was working on thermal management as a visiting researcher in microelectronic department of TU Delft and currently, he continues as a postdoc researcher.

Hamid Saffari received his Ph.D. degree from Moscow Power Engineering Institute, Russia. He is currently an Associate Professor at the School of Mechanical Engineering at Iran University of Science and Technology. His research interests include two-phase flow and HVAC&R.

Guo Qi Zhang is an IEEE fellow and Chair Professor for Micro/Nanoelectronics System Integration and Reliability in TU Delft. He has authored/co-authored more than 300 scientific publications; chaired/co-chaired several international conferences; and serves as associate editor for three international journals.

References

[1] D. E. Kim, D. I. Yu, D. W. Jerng, M. H. Kim, and H. S. Ahn, "Review of boiling heat transfer enhancement on micro/nanostructured surfaces," *Exp. Therm. Fluid Sci.*, vol. 66, pp. 173–196, 2015. DOI: 10.1016/j.expthermflusci.2015.03.023.

[2] J. Kim, S. Jun, R. Laksnarain, and S. M. You, "Effect of surface roughness on pool boiling heat transfer at a heated surface having moderate wettability," *Int. J. Heat Mass Transfer*, vol. 101, pp. 992–1002, 2016. DOI: 10.1016/j.ijheatmasstransfer.2016.05.067.

[3] S. W. Ahmad, J. S. Lewis, R. J. McGlen, and T. G. Karayiannis, "Pool boiling on modified surfaces using R-123," *Heat Transfer Eng.*, vol. 35, pp. 1491–1503, 2014. DOI: 10.1080/01457632.2014.889493.

[4] H. T. Phan, N. Caney, P. Marty, S. Colasson, and J. Gavillet, "Surface wettability control by nanocoating: the effects on pool boiling heat transfer and nucleation mechanism," *Int. J. Heat Mass Transfer*, vol. 52, pp. 5459–5471, 2009. DOI: 10.1016/j.ijheatmasstransfer.2009.06.032.

[5] E. Teodori, T. Palma, T. Valente, A. S. Moita, and A. L. Moreira, "Bubble dynamics and heat transfer for pool boiling on hydrophilic, superhydrophobic and biphilic surfaces," *J. Phys.: Conference Series*, vol. 745, pp. 032132–8, 2016.

[6] S. Sarangi, J. A. Weibel, and S. V. Garimella, "Quantitative evaluation of the dependence of pool boiling heat transfer enhancement on sintered particle coating characteristics," *J. Heat Transfer*, vol. 139, pp. 021502–13, 2016. DOI: 10.1115/1.4034901.

[7] S. J. Thiagarajan, R. Yang, C. King, and S. Narumanchi, "Bubble dynamics and nucleate pool boiling heat transfer on microporous copper surfaces," *Int. J. Heat Mass Transfer*, vol. 89, pp. 1297–1315, 2015. DOI: 10.1016/j.ijheatmasstransfer.2015.06.013.

[8] H. O'Hanley et al. "Separate effects of surface roughness, wettability, and porosity on the boiling critical heat flux," *Appl. Phys. Lett.*, vol. 103, pp. 024102–5, 2013. DOI: 10.1063/1.4813450.

[9] M.-C. Lu, C.-H. Huang, C.-T. Huang, and Y.-C. Chen, "A modified hydrodynamic model for pool boiling CHF considering the effects of heater size and nucleation site density," *Int. J. Therm. Sci.*, vol. 91, pp. 133–141, 2015. DOI: 10.1016/j.ijthermalsci.2015.01.011.

[10] D. E. Kim, D. I. Yu, S. C. Park, H. J. Kwak, and H. S. Ahn, "Critical heat flux triggering mechanism on micro-structured surfaces: coalesced bubble departure frequency and liquid furnishing capability," *Int. J.*

Heat Mass Transfer, vol. 91, pp. 1237–1247, 2015. DOI: 10.1016/j.ijheatmasstransfer.2015.08.065.

[11] S. G. Kandlikar, "Controlling bubble motion over heated surface through evaporation momentum force to enhance pool boiling heat transfer," *Appl. Phys. Lett.*, vol. 102, pp. 051611–6, 2013. DOI: 10.1063/1.4791682.

[12] K.-H. Chu, R. Enright, and E. N. Wang, "Structured surfaces for enhanced pool boiling heat transfer," *Appl. Phys. Lett.*, vol. 100, pp. 241603–4, 2012. DOI: 10.1063/1.4724190.

[13] D. E. Kim, S. C. Park, D. I. Yu, M. H. Kim, and H. S. Ahn, "Enhanced critical heat flux by capillary driven liquid flow on the well-designed surface," *Appl. Phys. Lett.*, vol. 107, pp. 023903–5, 2015. DOI: 10.1063/1.4926971.

[14] B. S. Kim, H. Lee, S. Shin, G. Choi, and H. H. Cho, "Interfacial wicking dynamics and its impact on critical heat flux of boiling heat transfer," *Appl. Phys. Lett.*, vol. 105, pp. 191601-1–191601-4, 2014. DOI: 10.1063/1.4901569.

[15] N. S. Dhillon, J. Buongiorno, and K. K. Varanasi, "Critical heat flux maxima during boiling crisis on textured surfaces," *Nat. Communications*, vol. 6, no. 8247, pp. 12, 2015.

[16] Y.-W. Lu and S. G. Kandlikar, "Nanoscale surface modification techniques for pool boiling enhancement—a critical review and future directions," *Heat Transfer Eng.*, vol. 32, pp. 827–842, 2011. DOI: 10.1080/01457632.2011.548267.

[17] C. M. Patil and S. G. Kandlikar, "Review of the manufacturing techniques for porous surfaces used in enhanced pool boiling," *Heat Transfer Eng.*, vol. 35, pp. 887–902, 2014. DOI: 10.1080/01457632.2014.862141.

[18] R. P. Rioux, E. C. Nolan, and C. H. Li, "A systematic study of pool boiling heat transfer on structured porous surfaces: from nanoscale through microscale to macroscale," *AIP Advances*, vol. 4, pp. 117133–9, 2014. DOI: 10.1063/1.4902343.

[19] K.-H. Chu, Y. S. Joung, R. Enright, C. R. Buie, and E. N. Wang, "Hierarchically structured surfaces for boiling critical heat flux enhancement," *Appl. Phys. Lett.*, vol. 102, pp. 151602–5, 2013. DOI: 10.1063/1.4801811.

[20] A. Nazari and S. Saedodin, "Critical heat flux enhancement of pool boiling using a porous nanostructured coating," *Exp. Heat Transfer*, vol. 30, no. 4, pp. 316–327, 2016. DOI: 10.1080/08916152.2016.1249806.

[21] C. M. Patil, S. V. Santhanam, and S. G. Kandlikar, "Development of a two-step electrodeposition process for enhancing pool boiling," *Int. J. Heat Mass Transfer*, vol. 79, pp. 989–1001, 2014. DOI: 10.1016/j.ijheatmasstransfer.2014.08.062.

[22] P. Xu, Q. Li, and Y. Xuan, "Enhanced boiling heat transfer on composite porous surface," *Int. J. Heat Mass Transfer*, vol. 80, pp. 107–114, 2015. DOI: 10.1016/j.ijheatmasstransfer.2014.08.048.

[23] S. Li, R. Furberg, M. S. Toprak, B. Palm, and M. Muhammed, "Nature-inspired boiling enhancement by novel nanostructured macroporous surfaces," *Adv. Funct. Mater.*, vol. 18, pp. 2215–2220, 2008. DOI: 10.1002/adfm.200701405.

[24] Y. Tang et al. "Pool-boiling enhancement by novel metallic nanoporous surface," *Exp. Therm. Fluid Sci.*, vol. 44, pp. 194–198, 2013. DOI: 10.1016/j.expthermflusci.2012.06.008.

[25] M. Tetreault-Friend et al. "Critical heat flux maxima resulting from the controlled morphology of nanoporous hydrophilic surface layers," *Appl. Phys. Lett.*, vol. 108, pp. 243102–7, 2016. DOI: 10.1063/1.4954012.

[26] J. Gao, L.-S. Lu, J.-W. Sun, X.-K. Liu, and B. Tang, "Enhanced boiling performance of a nanoporous copper surface by electrodeposition and heat treatment," *Heat and Mass Transfer*, vol. 53, pp. 947–958, 2016. DOI: 10.1007/s00231-016-1868-4.

[27] L. Lu et al. "A novel in-situ nanostructure forming route and its application in pool-boiling enhancement," *Exp. Therm. Fluid Sci.*, vol. 72, pp. 140–148, 2016. DOI: 10.1016/j.expthermflusci.2015.11.005.

[28] A. M. Gheitaghy, H. Saffari, D. Ghasimi, and A. Ghasemi, "Effect of electrolyte temperature on porous electrodeposited copper for pool boiling enhancement," *Appl. Therm. Eng.*, vol. 113, pp. 1097–1106, 2017. DOI: 10.1016/j.applthermaleng.2016.11.106.

[29] A. M. Gheitaghy, H. Saffari, and M. Mohebbi, "Investigation pool boiling heat transfer in U-shaped mesochannel with electrodeposited porous coating," *Exp. Therm. Fluid Sci.*, vol. 76, pp. 87–97, 2016. DOI: 10.1016/j.expthermflusci.2016.03.011.

[30] H. S. Ahn, C. Lee, J. Kim, and M. H. Kim, "The effect of capillary wicking action of micro/nano structures on pool boiling critical heat flux," *Int. J. Heat Mass Transfer*, vol. 55, pp. 89–92, 2012. DOI: 10.1016/j.ijheatmasstransfer.2011.08.044.

[31] M. M. Rahman, E. Ölçeroğlu, and M. McCarthy, "Role of wickability on the critical heat flux of structured superhydrophilic surfaces," *Langmuir*, vol. 30, pp. 11225–11234, 2014. DOI: 10.1021/la5030923.

[32] C.-K. Guan, B. Bon, J. Klausner, and R. Mei, "Comparison of CHF enhancement on microstructured surfaces with a predictive model," *Heat Transfer Eng.*, vol. 35, pp. 452–460, 2014. DOI: 10.1080/01457632.2013.833043.

[33] S. G. Kandlikar, "A theoretical model to predict pool boiling CHF incorporating effects of contact angle and orientation," *J. Heat Transfer*, vol. 123, pp. 1071–1079, 2001. DOI: 10.1115/1.1409265.

[34] N. D. Nikolic, L. J. Pavlovic, M. G. Pavlovic, and K. I. Popov, "Effect of temperature on the electrodeposition of disperse copper deposits," *J. Serb. Chem. Soc.*, vol. 72, no. 12, pp. 1369–1381, 2007. DOI: 10.2298/JSC0712369N.

[35] W. M. Rohsenow, "A method of correlating heat transfer data for surface boiling of liquids," *Trans. ASME*, vol. 74, pp. 969–976, 1952.